



Modeling of the marine circulations and contamination by wastewater in the Nador lagoon

A. Yachouti¹, Y. Lakhlifi¹, S. Daoudi², I. Elmahi¹

¹Laboratoire de Mécanique et Modélisation Numérique, ENSAO, Université Mohammed I, Oujda, Maroc.

²Laboratoire de Mécanique et Energétique, FSO, Université Mohammed I, Oujda, Maroc.

Received 11 Jan 2018,
Revised 08 Apr 2018,
Accepted 01 May 2018

Keywords

- ✓ Shallow water,
- ✓ Finite volume,
- ✓ SRNH solver,
- ✓ Water recirculation.
- ✓ Wastewater,
- ✓ Nador lagoon.

imelmahi@gmail.com
Phone: +212663042319

Abstract

In this paper, marine circulations and transport of wastewater in the Nador lagoon, considering the new inlet with Mediterranean Sea, are simulated by the finite volume method. The physical model is based on the well known 2D shallow water equations that include slope variations and friction losses. Convection fluxes are approximated by a second order Non Homogeneous Riemann Solver (SRNH) on unstructured meshes, whereas an operator splitting procedure is used for the friction terms. The solver can be applied to model flows on complicated geometries and can handle slope variations while preserving the balance between the pressure gradient and the bed source term. Results show clearly the presence of recirculation zones inside the lagoon. In addition, it is found that the flow is almost inert at Beni Enzar and Kariat Arkmane which leads to a contamination and a stagnation of the wastewater in these regions.

1. Introduction

Lagoons are almost closed bodies connected loosely to the sea by narrow channels subjected to siltation and sediment obstruction. The hydrodynamic circulation pattern of these bodies is difficult to compute due to their usually complex geometry combined with the influence of the tides, the wind and the fresh water inputs coming from the rivers and streams of the lagoon watershed. From a biological point of view, lagoons can be characterized as complex ecosystems in a fragile equilibrium and their modelling is a difficult task as one has to take into account numerous interactions between physical, chemical and biological parameters.

Lagoons have important environmental and societal aspects. They are extremely rich from a biological point of view as the reproduction area of a great number of species as well as the passage of many migratory bird species. Lagoons are also the siege of many human activities: urbanization, tourism, agriculture, fishing and shell-fishing farming all influencing the lagoon state in a complex way. Many lagoons are affected over the years by anthropogenic influences, including environmental degradation and local or global sources of pollution. Among these lagoons, the Nador lagoon located on the North-East of Morocco is an ecosystem that is of great biological, ecological and economic interest. It covers an area that exceeds 120 Km² and a maximum depth of 8m and is fed by water of the Mediterranean through a pass known as 'Bokhana', the freshwater waterways, the rejections of the untreated human activities (agriculture and urban water industry, metallurgy, textile ...), and by water of the station of purification. Figure 1, taken from [1], gives a Schematic description of the Nador lagoon.

Ecological qualities of the lagoon have been relatively affected, during the last years, by the human activities, particularly the pollution coming from worn water of the city and the waste evacuated along its banks as well as the hydrocarbons coming from the industrial boats. These polluting products, if they are not rapidly evacuated, could have a harmful effect on humans. This is manifested in damage to biological resources, risks for human health, deterioration of marine activities including fishing, the quality of seawater. In addition, the Nador lagoon has been the subject of many recent investigations that have concerned water quality, currents, bathymetry, flora, fauna, fishing and aquaculture (see for instance [2-4]). These studies have focused especially on the environmental aspect of the lagoon and are biological, geochemical and economic ([5,6]). However, the

studies from numerical point of view concerning the transport and dispersion of contaminants in the surroundings of the lagoon are missing. The rare works in the literature on the subject can be found in ([7], [8]). Using numerical models it is possible now to predict changes in water quality and to plan suitable interventions and control strategies for environmental protection.

In this paper, we propose a finite volume method for the simulation of the hydrodynamic, water circulations and transport of wastewater in the Nador lagoon. The physical model is based on the 2D shallow water equations that include slope variations and friction terms. The computational code uses a Non Homogeneous Riemann Solver (SRNH) for the discretization of the convection and bed slope source terms [9], and semi-implicit splitting scheme for the friction terms. It can be used on complicated geometries by incorporating unstructured meshes. In addition, the algorithm preserves the balance between the pressure gradient and source term due to the slope variation. The preliminary results that will be presented here considering the new “pass” with the Mediterranean Sea, will demonstrate the performance and robustness of the solver for the simulation of flows in real situations.

The paper is organized as follows. The governing equations are first described in section 2. This includes the equations for the free-surface flow and the model for pollutant transport and dispersion. Section 3 is devoted to the solution procedure for the proposed model. We describe the finite volume discretization and the formulation of the SRNH scheme on unstructured grids. The extension to second order and the treatment of the friction terms are also shown. In section 4, we present an application of the solver to the simulation of the hydrodynamic circulations and a wastewater transport event in the Nador lagoon. Some concluding remarks are given in section 5.

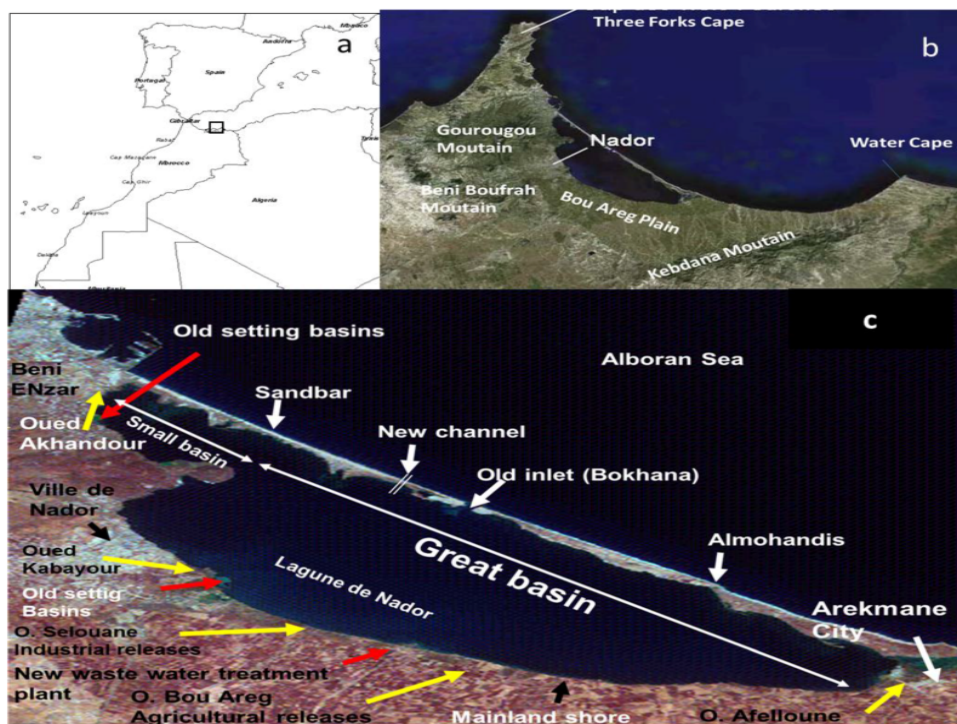


Figure 1: Maps showing Nador lagoon location (a) Lagoon watershed (b) and lagoon and freshwater hydrographic network (shown by yellow arrows), old settling basins and new wastewater treatment plant (shown by red arrows) (c) [1].

2. The equations to be solved

The mathematical model can be derived by vertical integration of the three-dimensional incompressible Navier-Stokes equations along with the assumptions of a hydrostatic pressure and a vertically uniform horizontal velocity field, which results in the well-established shallow water equations written in conservative form as

$$\frac{\partial W}{\partial t} + \frac{\partial}{\partial x} (F(W) - \tilde{F}(W)) + \frac{\partial}{\partial y} (G(W) - \tilde{G}(W)) = S_1(W) + S_2(W) \quad (1)$$

W is the vector of conserved variables, S_1 and S_2 are the source terms due to slope variations and friction forces, F and G are the advection tensor fluxes \tilde{F} and \tilde{G} are the diffusion tensor fluxes

$$W = \begin{pmatrix} h \\ hu \\ hv \\ hC \end{pmatrix}; \quad F(W) = \begin{pmatrix} hu \\ hu^2 + \frac{1}{2}gh^2 \\ huv \\ huC \end{pmatrix}; \quad G(W) = \begin{pmatrix} hv \\ huv \\ hv^2 + \frac{1}{2}gh^2 \\ hvC \end{pmatrix}$$

$$\tilde{F}(W) = \begin{pmatrix} 0 \\ 0 \\ 0 \\ D_x \partial_x (hC) \end{pmatrix}; \quad \tilde{G}(W) = \begin{pmatrix} 0 \\ 0 \\ 0 \\ D_y \partial_y (hC) \end{pmatrix}; \quad S_1(W) = \begin{pmatrix} 0 \\ ghS_{ox} \\ ghS_{oy} \\ 0 \end{pmatrix}; \quad S_2(W) = \begin{pmatrix} 0 \\ -ghS_{fx} \\ -ghS_{fy} \\ hQ \end{pmatrix}$$

g is the gravitational acceleration, h is the water depth, u and v are the depth-averaged velocities in the x and y direction respectively. The bed slopes are functions of the bottom level Z and are given by

$$S_{ox} = -\frac{\partial Z}{\partial x}; \quad S_{oy} = -\frac{\partial Z}{\partial y},$$

and the friction losses along the x and y direction are described in terms of the Manning's roughness coefficient n_b :

$$S_{fx} = \frac{n_b^2 u \sqrt{u^2 + v^2}}{h^3}; \quad S_{fy} = \frac{n_b^2 v \sqrt{u^2 + v^2}}{h^3},$$

In the pollutant equation, C is the depth-averaged contaminant concentration, D_x and D_y the diffusion coefficient and Q the depth-averaged pollutant source or sink.

3. Numerical methods

3.1 Mesh generation and bed topography

Let Ω be the domain of computation covered by a conformal grid consisting of a set of unstructured polygons K that are as general as possible. In this work the unstructured meshes are composed of triangles. Figure 2 (left) shows the mesh of the Nador lagoon generated by using the Delaunay triangulation technique [10]. Since the boundary conditions in the Mediterranean part are not well known, the computational domain has been limited in this study to the pass between the lagoon and Mediterranean sea. In this way the tidal boundary conditions will be imposed at this pass.

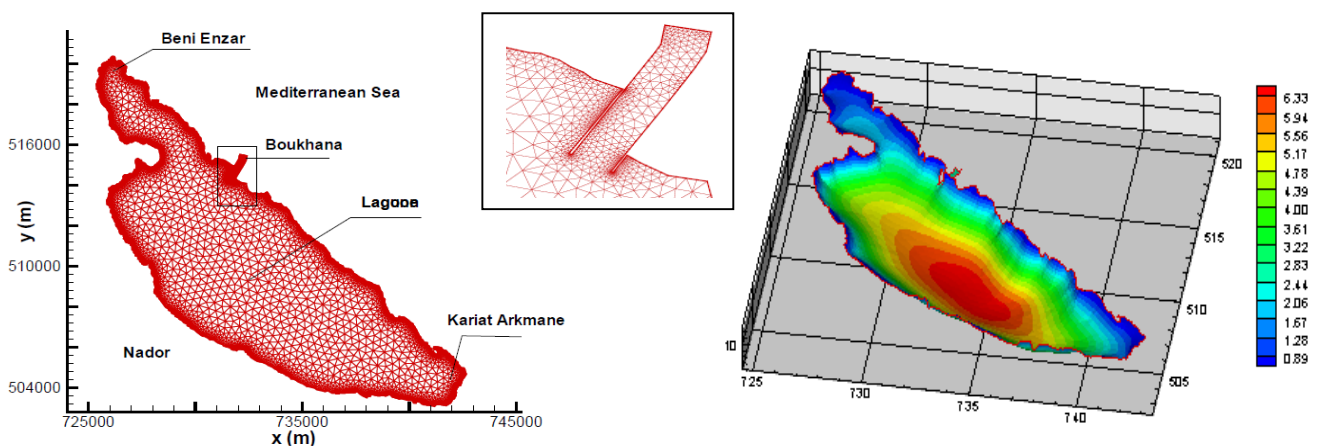


Figure 2: Unstructured mesh of the Nador lagoon (left), zoom on the “pass” (middle) and Bathymetry (right).

The geometry and the bed surface topography of the lagoon are very irregular and several regions of various depths coexist. In our simulations the bathymetry was reconstructed from topographical data. This bathymetry is illustrated in Figure 2 (right).

3.2 Finite volume formulation

Research on numerical solution of equations (1) has received considerable attention during the last decades and a several finite volume methods have been developed, compare [11,12] among others. The main advantages of

these methods lie on their implementation on unstructured triangular meshes and preserving conservation properties of the equations. The computational code developed here uses the «cell-centred» finite volume formulation for which all the state variables are updated at the centroid of each cell (the centre of gravity in our case). Figure 3 illustrates the type of control volumes used.

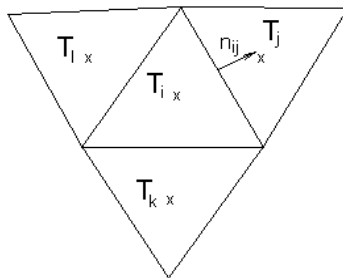


Figure 3: A cell-centred control volume.

Hence, integration of the system (1) over a control volume T_i and using Gauss divergence, an explicit finite volume discretization yields to

$$W_i^{n+1} = W_i^n - \frac{\Delta t}{|T_i|} \left[\sum_{j \in N(i)} \int_{\Gamma_{ij}} H(W^n, n) d\sigma - \sum_{j \in N(i)} \int_{\Gamma_{ij}} \tilde{H}(W^n, n) d\sigma - \int_{T_i} S_1(W^n) dV - \int_{T_i} S_2(W^n) dV \right] \quad (2)$$

where the convection and diffusion flux functions are defined by

$$H(W, n) = F(W)n_x + G(W)n_y \quad ; \quad \tilde{H}(W, n) = \tilde{F}(W)n_x + \tilde{G}(W)n_y$$

$N(i)$ is the set of neighboring triangles of the cell T_i , W_i^n is an average value of the solution W in the cell T_i at time t^n , Γ_{ij} is the edge separating control volumes T_i and T_j , and $n = (n_x, n_y)^T$ denotes the unit vector normal to Γ_{ij} .

3.3 Discretization of the convective and bed slope source terms

The system of Saint-Venant equations (1) includes the variation of topography and therefore special attention should be paid to his numerical discretization. Indeed, a well known problem is that shallow-water equations on non-flat topography have steady-state solutions in which the flux gradients are non zero but are exactly balanced by the source terms. Standard numerical methods for the discretization of conservation laws may fail in correctly reproducing this balance (called also C-property) and, thus, specific methods have been developed to deal with this problem (well-balanced schemes, see e.g., [13,14]). The method adopted herein for the space discretization has been proposed by Benkhaldoun, Elmahi and Seaid in a series of papers (see for instance [9, 15, 16]). It is based on a Riemann Solver, named SRNH, and consists of a predictor stage for which the state W_{ij} at each edge Γ_{ij} is computed by solving a Riemann problem, and a corrector stage where the state W^{n+1} at time t^{n+1} is reconstructed iteratively using the physical flux on W_{ij} . The scheme considers only the advection part and the source term containing slope variations

$$\frac{\partial W}{\partial t} + \frac{\partial F(W)}{\partial x} + \frac{\partial G(W)}{\partial y} = S_1(W) \quad (3)$$

Let's start with the predictor stage. A projection of the system (3) according to the normal η and tangential τ yields:

$$\begin{cases} \frac{\partial h}{\partial t} + \frac{\partial(hu_\eta)}{\partial \eta} = 0 \\ \frac{\partial(hu_\eta)}{\partial t} + \frac{\partial(hu_\eta^2 + \frac{1}{2}gh^2)}{\partial \eta} = -gh \frac{\partial Z}{\partial \eta} \\ \frac{\partial(hu_\tau)}{\partial t} + \frac{\partial(hu_\eta u_\tau)}{\partial \eta} = 0 \\ \frac{\partial(hC)}{\partial t} + \frac{\partial(hu_\eta C)}{\partial \eta} = 0 \end{cases} \quad (4)$$

where $u_\eta = un_x + vn_y$ and $u_\tau = -un_y + vn_x$ are, respectively, the normal and tangential velocity.

For this projected system, the predictor stage is then formulated, for the evaluation of the averaged state U_{ij}^n on each edge Γ_{ij} , using an upwind scheme, in the following manner

$$U_{ij}^n = \frac{1}{2}(U_i^n + U_j^n) - \frac{1}{2} \operatorname{sgn}[\nabla F_\eta(\bar{U})](U_j^n - U_i^n) + \frac{1}{2} |\nabla F_\eta(\bar{U})^{-1}| S_{lij}^n \quad (5)$$

$$U = \begin{pmatrix} h \\ hu_\eta \\ hu_\tau \\ hC \end{pmatrix}, \quad F_\eta(U) = \begin{pmatrix} hu_\eta \\ hu_\eta^2 + \frac{1}{2}gh^2 \\ hu_\eta u_\tau \\ hu_\eta C \end{pmatrix}, \quad S_{lij}^n = -g \frac{h_i + h_j}{2} (Z_j - Z_i) \begin{pmatrix} 0 \\ 1 \\ 0 \\ 0 \end{pmatrix}$$

In (5), \bar{U} is the intermediate Roe-averaged state given by

$$\bar{U} = \frac{1}{2}(h_i + h_j) \begin{pmatrix} 1 \\ \frac{u_i \sqrt{h_i} + u_j \sqrt{h_j}}{\sqrt{h_i} + \sqrt{h_j}} n_x + \frac{v_i \sqrt{h_i} + v_j \sqrt{h_j}}{\sqrt{h_i} + \sqrt{h_j}} n_y \\ -\frac{u_i \sqrt{h_i} + u_j \sqrt{h_j}}{\sqrt{h_i} + \sqrt{h_j}} n_y + \frac{v_i \sqrt{h_i} + v_j \sqrt{h_j}}{\sqrt{h_i} + \sqrt{h_j}} n_x \\ \frac{C_i \sqrt{h_i} + C_j \sqrt{h_j}}{\sqrt{h_i} + \sqrt{h_j}} \end{pmatrix}$$

$\operatorname{sgn}[\nabla F_\eta(\bar{U})]$ denotes the sign matrix of the Jacobean $\nabla F_\eta(\bar{U})$, it is defined by:

$$\operatorname{sgn}[\nabla F_\eta(\bar{U})] = R(\bar{U}) \operatorname{sgn}[\Lambda(\bar{U})] R^{-1}(\bar{U}) \quad \text{and} \quad |\nabla F_\eta(\bar{U})^{-1}| = R(\bar{U}) |\Lambda(\bar{U})^{-1}| R^{-1}(\bar{U})$$

$R(\bar{U})$ and $\Lambda(\bar{U})$ are respectively the eigenvector and eigenvalue matrices of $\nabla F_\eta(\bar{U})$.

By incorporating these matrices in the predictor stage (5), the projected state U_{ij}^n on each edge Γ_{ij} can be easily obtained. The conservative state W_{ij}^n is then evaluated using the transformations $u = u_\eta n_x - u_\tau n_y$ and $v = u_\eta n_y + u_\tau n_x$.

Therefore, the incremental corrector stage is written using the non projected conservative states in the following manner:

$$W_i^{n+1} = W_i^n - \frac{\Delta t}{|T_i|} \sum_{j \in \mathcal{N}(i)} H(W_{ij}^n; n_{ij}) |\Gamma_{ij}| + \Delta t S_i^n \quad (6)$$

$|T_i|$ is the surface of the control volume T_i and $|\Gamma_{ij}|$ the length of the edge Γ_{ij} separating triangles T_i and T_j

In the corrector stage (6), the source term approximation is reconstructed in such a way to obtain a well balanced scheme preserving steady state at rest (see [9] for details on this reconstruction).

3.4 Second order well-balanced scheme

The SRNH scheme described above is first order accurate in space. It is monotone but has a poor accuracy due to the large amount of numerical dissipation. The extension to 2nd-order accuracy in space can be achieved by using a classical MUSCL technique [9]. In the definition of the flux in (6), we replace the piecewise constant values W_i and W_j by more accurate reconstructions deduced from piecewise linear approximations, namely the values W_{ij} and W_{ji} , reconstructed on both sides of the interface as follow

$$\begin{cases} W_{ij} = W_i + \frac{1}{2} \left(\beta \nabla W_i \cdot X_i \vec{X}_j + (1 - \beta)(W_j - W_i) \right) \\ W_{ji} = W_j - \frac{1}{2} \left(\beta \nabla W_j \cdot X_j \vec{X}_i + (1 - \beta)(W_j - W_i) \right) \end{cases} \quad (7)$$

where ∇ denotes the gradient operator, $X_i = (x_i, y_i)^T$ and $X_j = (x_j, y_j)^T$ are respectively the barycentres of cells T_i and T_j . β is a parameter between 0 and 1. In practice one uses $\beta = 2/3$. The resulting scheme is

second order in space but is not necessarily monotonous and non-physical oscillations are produced. To damp the numerical oscillations in the current computations, the Van Albada flux limiter is applied:

$$\begin{cases} W_{ij} = W_i + \frac{1}{2} \lim \left(\beta \nabla W_i \cdot X_i \vec{X}_j + (1 - \beta)(W_j - W_i) W_j - W_i \right) \\ W_{ji} = W_j - \frac{1}{2} \lim \left(\beta \nabla W_j \cdot X_j \vec{X}_i + (1 - \beta)(W_j - W_i) W_j - W_i \right) \end{cases} \quad (8)$$

with the Van albada limiter given by

$$\begin{cases} \lim(a, b) = \frac{(a^2 + \varepsilon)b + (b^2 + \varepsilon)a}{a^2 + b^2 + 2\varepsilon} & \text{if } ab > 0 \\ \lim(a, b) = 0 & \text{otherwise} \end{cases}$$

where $0 < \varepsilon \ll 1$. With this limitation one obtains a monotonic second reconstruction for the hyperbolic part.

3.5 Treatment of the friction terms

The friction terms in (2) are discretized using an operator splitting procedure. For example, to evaluate the x -momentum, the second equation of the system (2) is split into two equations

$$\begin{cases} \frac{\partial hu}{\partial t} = -n_b^2 g u \frac{\sqrt{u^2 + v^2}}{h^{\frac{1}{3}}} \\ \frac{\partial hu}{\partial t} + \text{Res}(W) = -gh \frac{\partial Z}{\partial x} \end{cases} \quad (9)$$

where n_b is the Manning's coefficient and Res describes the convection contributions in the x -momentum equation corresponding to the surface integral in eq. (2), and is approximated as the sum taken over all boundary segments.

First, a semi-implicit method is used to integrate the upper equation in (7), giving

$$\frac{(\hat{hu})_i - (hu)_i^n}{\Delta t} = -n_b^2 g (hu)_i \frac{\sqrt{(u_i^n)^2 + (v_i^n)^2}}{(h_i^n)^{\frac{4}{3}}} \quad (10)$$

In the second step, the value $(\hat{hu})_i$ is taken to be the initial condition when solving the second equation in (9).

3.6 Discretization of the diffusion terms

Finally, to approximate the diffusion fluxes in the discrete system (2) a Green-Gauss diamond reconstruction is used here, see for example [17] and further references are therein. This method has been selected because it is second-order accurate, it can be applied on general unstructured grids, it does not require serious restrictions on the angles of triangles, and it can be easily incorporated in our finite volume scheme. Hence, a co-volume coV_{ij} is first constructed by connecting the barycentre of the elements that share the edge Γ_{ij} and its endpoints as shown in Figure (4) below.

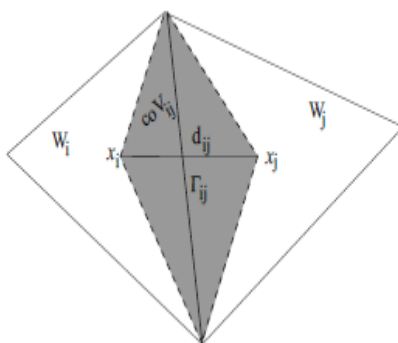


Figure 4: A generic control volume and notations.

Then, the diffusion fluxes in the concentration equation are evaluated at an inner edge Γ_{ij} as

$$\int_{\Gamma_i} \frac{\partial}{\partial x} \left(D_x h \frac{\partial C}{\partial x} \right) dV = \frac{D_x h|_{\Gamma_{ij}}}{|coV_{ij}|} \sum_{\varepsilon \in \partial coV_{ij}} \frac{C_{N_1} + C_{N_2}}{2} \int_{\varepsilon} n_x d\sigma \quad (11)$$

where N_1 and N_2 are the nodes of the edge ε on the surface ∂coV_{ij} , C_{N_1} and C_{N_2} are the values of the pollutant concentrations at the nodes N_1 and N_2 respectively.

4. Numerical tests

3.1 Hydrodynamic in the Nador lagoon

The first test case that we consider here consists is the study of the hydrodynamic and water circulations in the Nador lagoon. This test problem is interesting in the sense that it can give an answer to how the water moves into the lagoon, regions where the water recirculates and those where it stagnates. These last regions can be in fact very affected by contamination of wastewater coming from the city. The computations can also give an idea of the time residence of the water coming from the Mediterranean Sea before leaving the entrance of the lagoon. Initially, the flow is assumed to be at rest with constant free surface ($h + Z = Cte$).

Two types of boundary conditions must be specified respectively at the pass between the Mediterranean Sea and the lagoon noted Γ_p and land-type boundary located on the Nador coastlines Γ_w . Hence the following boundary conditions :

$$\nabla u \cdot n = 0 \quad \text{on } \Gamma_p \text{ and } \Gamma_w$$

are imposed for the water flow and

$$h = H + h_0 + A_* \cos(\omega_* t + \varphi_*) \quad \text{on } \Gamma_p \quad (12)$$

$$\nabla h \cdot n = 0 \quad \text{on } \Gamma_p$$

are used for the water height.

In (12), H is the depth from a fixed reference level to the bottom, h_0 is a given averaged water elevation taken here equal to $3m$ (initially we have $h=H+ h_0$), A_* is the tidal amplitude at the entrance of the lagoon, ω_* is the angular frequency of the tide, and φ_* is the phase of the tide. In the Nador lagoon, the main astronomical tidal constituents are the semidiurnal M_2 , S_2 and N_2 tides, and the diurnal K_1 tide. The values of the parameters A_* , ω_* and φ_* for each tidal wave are taken from [18] and are illustrated in table 1. Thus, the boundary condition on Γ_p is replaced by

$$h = H + h_0 + A_{M_2} \cos(\omega_{M_2} t + \varphi_{M_2}) + A_{S_2} \cos(\omega_{S_2} t + \varphi_{S_2}) + A_{N_2} \cos(\omega_{N_2} t + \varphi_{N_2}) + A_{K_1} \cos(\omega_{K_1} t + \varphi_{K_1}) \quad (13)$$

Note that the boundary conditions for the water height on Γ_p are time-dependent and should be updated at each time step according to the condition (13).

Table 1: Parameters for the considered tidal waves at the ‘pass’ of the Nador Lagoon.

<i>Tide</i>	<i>A*[m]</i>	<i>ω*[rad/s]</i>	<i>φ*[°]</i>
M2	0.288	1.4052 10-4	-55.02
S2	0.105	1.4544 10-4	-76.13
N2	0.071	1.3788 10-4	-37.38
K1	0.038	7.2921 10-5	-147.72

The computations have been performed with a physical time step Δt chosen in such a way that the following stability condition is satisfied

$$\Delta t = CFL \cdot \min_{\Gamma_{ij}} \left(\frac{|T_i| + |T_j|}{2|\Gamma_{ij}| \max(|\lambda^p|_{ij})} \right)$$

where λ^p_{ij} is the eigenvalue of the system, evaluated at the interface Γ_{ij} between two cells T_i and T_j , and CFL is the courant number taken here equal to 0.5 in order to ensure stability of the numerical scheme. In the figure 5, is presented the water height inside the lagoon. The computations have been performed for 6 days in physical times.

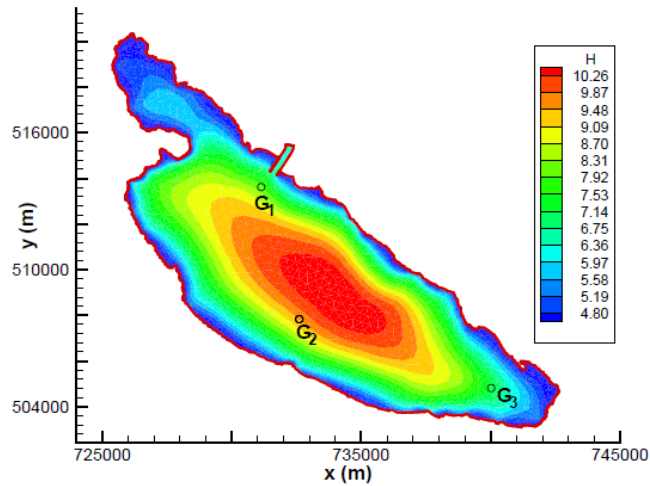


Figure 5: Water depth contours in the Nador lagoon at physical time $t = 24h$.

In Figures 6 and 7 respectively, are illustrated the velocity field together with the iso-lines of u-velocity in the case of high and low tides. The clear result is the presence of recirculation zones inside the lagoon. It is also clear that in case of high tides the water flow is coming from the Mediterranean part and feeds the lagoon, this can be clearly seen on the Figure 6. On the other hand, when the tides are low, the water flows from the lagoon toward the Mediterranean part (see Figure 7). One can also observe that the flow is almost inert at Beni Enzar and Kariat Arkmane regions. These regions could then be very affected in case of contamination by wastewater because the pollutant can stagnate in these regions.

In order to validate the results obtained by our solver, and since the observation data are missing, computations have been compared with those obtained by using the finite volume Vazquez solver which is based on a well balanced modified Roe scheme (see [13]). Figures 8, 9 and 10 show the historic of water depth and u-velocity with time at three gauged points, G_1 situated at the entrance near the “pass”, G_2 situated inside the lagoon and G_3 situated at Kariat Arkmane region where the flow is almost inert (see Figure 5).

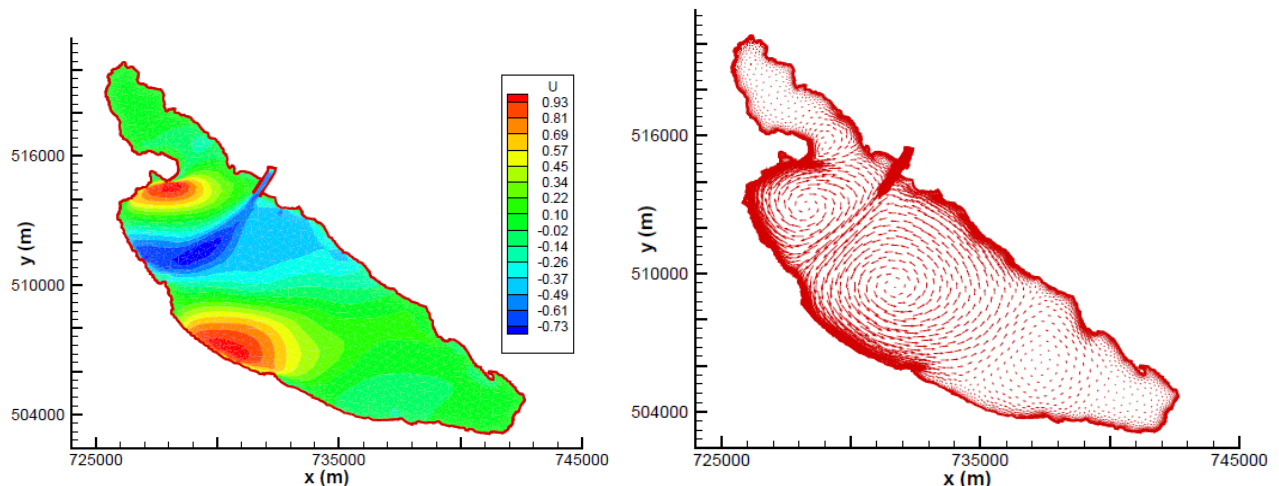


Figure 6: Velocity field (left) and iso-lines of u-velocity (right) in the case of high tides.

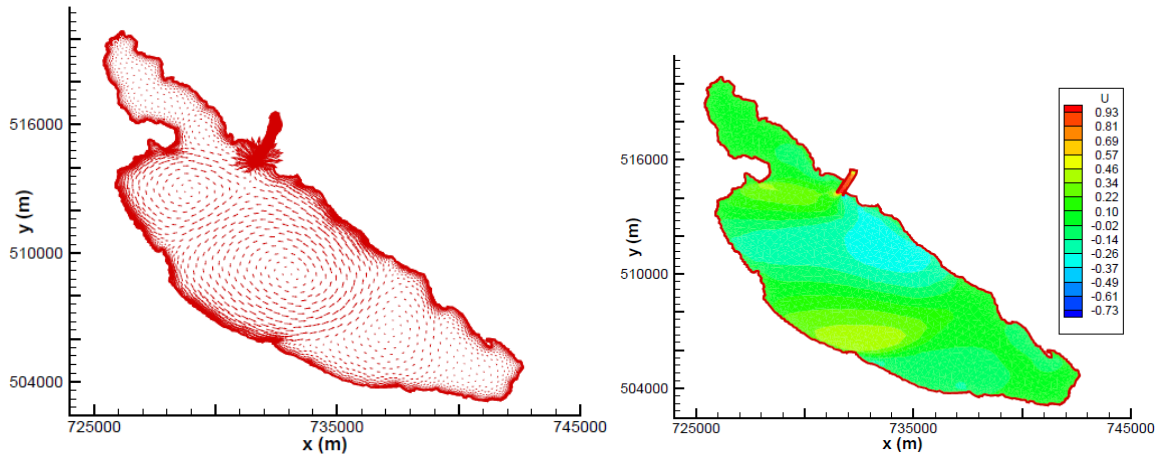


Figure 7: Velocity field (left) and iso-lines of u-velocity (right) in the case of low tides.

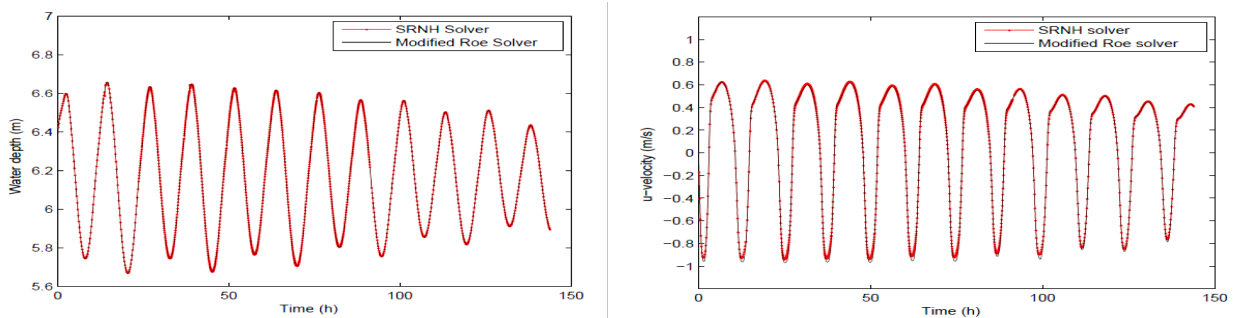


Figure 8: Water depth and u-velocity versus time at gauged point G_1

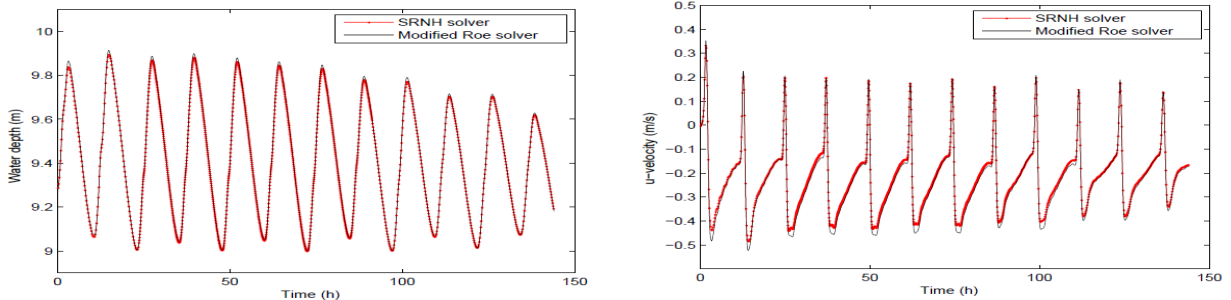


Figure 9: Water depth and u-velocity versus time at gauged point G_2

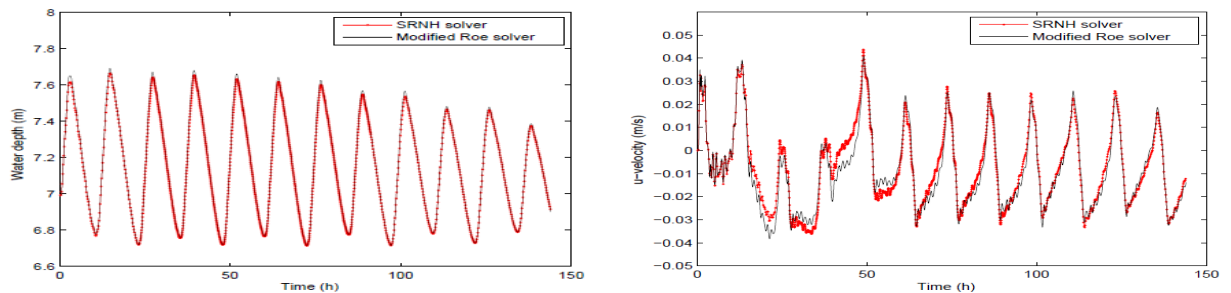


Figure 10: Water depth and u-velocity versus time at gauged point G_3

One remarks that the velocity is larger at the gauged point G_1 . This is due to the tide coming from the pass. The values of this velocity evolve from negative to positive depending on the case of high or low tides. Moreover, the negative and positive values of u-velocity at the gauged point G_2 can be explained by the hydrodynamic circulations in this zone. Finally, at the gauged point G_3 which is far from the tides and recirculation zones, we remark that the velocity is almost zero. One can notice also an excellent agreement between our results and

those obtained by the well known Vazquez finite volume solver, which confirms the capability of the finite volume solver developed here to deal with complicated geometries and real situations in shallow water flow.

3.2 Transport of wastewater in the Nador lagoon

As second validation test, we applied the solver for a contamination event in the Nador lagoon. The situation we consider here models the contamination by wastewater of the city. These wastewater are released from fifteen boundaries with discharge $Q = 1 \text{ m}^3/\text{s}$. The diffusion coefficients in x and y direction are taken constants $D_x = D_y = 10^{-5}$ and the Manning's coefficient $N = 10^{-3}$. For this test case, three types of boundary conditions are specified respectively at the “pass” between the Mediterranean Sea and the lagoon noted Γ_p , land-type boundary located on the Nador coastlines Γ_w , and the fifteen boundaries Γ_c from where the wastewater are released. These boundary conditions are shown in Figure 11 below. Hence the boundary conditions are:

$$\begin{aligned} \vec{U} \cdot n = 0, \quad \nabla C \cdot n = 0, \quad h = h_0 + A_{M2} \cos(\omega_{M2}t + \varphi_{M2}) + A_{S2} \cos(\omega_{S2}t + \varphi_{S2}) \\ + A_{N2} \cos(\omega_{N2}t + \varphi_{N2}) + A_{K1} \cos(\omega_{K1}t + \varphi_{K1}) \end{aligned} \quad \text{on } \Gamma_p$$

$$\vec{U} \cdot n = 0, \quad \nabla h \cdot n = 0, \quad \nabla C \cdot n = 0 \quad \text{on } \Gamma_w$$

$$Q = 1 \text{ m}^3/\text{s}, \quad \nabla h \cdot n = 0, \quad C = 1 \quad \text{on } \Gamma_c$$

It is also important to mention that the initial conditions have been obtained by simulating the hydrodynamic of shallow water equations for 6 days in physical times until the flow is established (see results of the test case 1). After that, the water height and the velocity field are taken as initial state. The period of the tides has been found to be of the order of 12 hours. Figure 12 shows the contour plots of wastewater concentration at a physical time of 10 days.

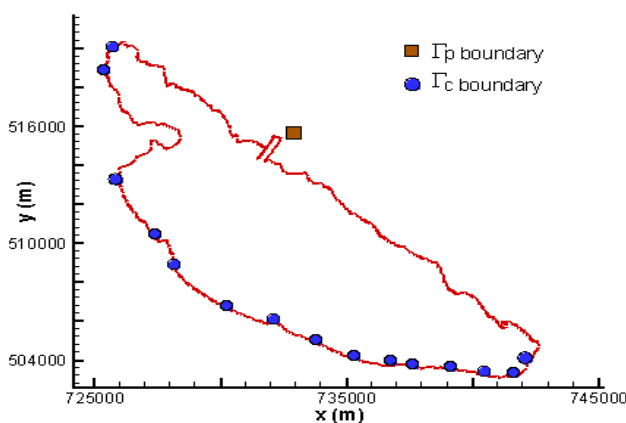


Figure 11: Imposed boundary conditions.

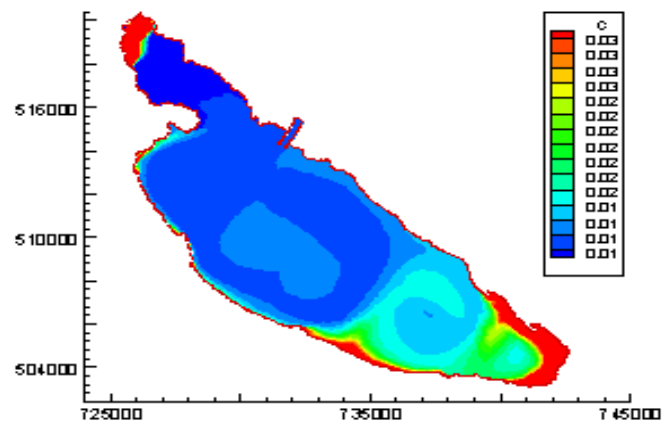


Figure 12: Wastewater dispersion in the Nador lagoon after a physical time of 10 days.

The pollutants coming from the fifteen boundaries are mixed and form some vortices inside the lagoon. This is due mainly to the recirculation in the hydrodynamic of the water inside the lagoon. The contaminant goes increasingly towards the “pass” in the direction of the Mediterranean part. It can be noted also in the legend of Figure 12 that the pollutant quantity that has been dispersed inside the lagoon is of the order 0.01, which is relatively low compared to the concentration released from the boundaries, but is significant to pollute the water in the lagoon.

Conclusion and perspectives

In this paper, a numerical code based on the finite volume method has been applied for the simulation of the hydrodynamic, water circulations and transport-dispersion of contaminant caused by wastewater in the Nador lagoon. The method consists of two stages, which can be interpreted as a predictor–corrector procedure. In the first stage, the scheme uses the projected system of the coupled equations and introduces the sign matrix of the flux Jacobian, which results in an upwind discretization of the characteristic variables. In the second stage, the solution is updated using the conservative form of the equations and a special treatment of the bed bottom to obtain a well-balanced discretization of the flux gradients and the source terms. The solver can be used on

complicated geometries with unstructured meshes. The tests cases presented here shows the good performance of the method and confirms its capability to provide accurate and efficient simulations for shallow water flows including complex topography and friction forces on unstructured grid.

As perspective, a relevant study would also measure the residence time of water coming from the Mediterranean Sea into the lagoon in order to find a way to renew it often, and thus make it less polluted. An adequate numerical study would determine the necessity and indeed the eventual location of another passes between the lagoon and the Mediterranean permitting to reduce the residence time of a given tracer.

References

1. N. M. Najih, D. Nachite, N. Berday, R. Pastres, A. Lamrini and N. Rezzoum, *J. Mar. Sci. Eng.*, 5(1) (2017) 1-18.
2. N.M. Idrissi, Y. Zahri., R. Houssa., B. Abdellaoui and N. El Ouamari, *Projet FAO- COPEM*, (2002).
3. F. Ruiz, M. Abad, E.X.M. Garcia, N. Hamoumi, M. Labraimi, E.H. Boumaggard and I. Bouamterhane, *Geo-Temas*, 6 (2004) 307-310.
4. M. Najih, N. Berday, A. Lamrini, D. Nachite, Y. Zahri, *Rev. Mar. Sci. Agron. Vét.*, 3 (1) (2015) 19-30.
5. N. Hammoumi, *Revue Paralia*, 5 (2012).
6. B. Abdellaoui, B. Nhhala, E.M. Talbaoui, *General Fisheries Commission for the Mediterranean*, N° 95, Rome, (2015).
7. K. Hilmi, A. Makaoui, M. Idrissi, B. Abdellaoui, Z. El Ouehadi, *Eur. Sci. J.*, 11 (2015) 418-428.
8. F. Benkhaldoun, S. Daoudi, I. Elmahi and M. Seaid, *Int. J. Math. Stat.* 8 (2011), 1-8.
9. F. Benkhaldoun, I. Elmahi and M. Seaid, *Comput. Methods Appl. Mech. Eng.* 199 (2010) 3324-3335.
10. F. Hermeline, PhD Thesis, Université Paris 6, (1980).
11. F. Alcrudo and P. Garcia-Navarro, *Int. J. Numer. Meth. Fluids*, 16 (1993) 489-505.
12. J.M Hervouet, in *J.M. Hervouet and P. Bates, Special Issue: The TELEMAC Modelling System*, 13 (2000).
13. M.E. Vazquez-Cendon, *J. Comput. Phys.*, 148 (1999) 497-526.
14. S. Noelle, N. Pankratz., G. Puppo and J.R. Natvig, *J. Comput. Phys.*, 213 (2006) 474-499.
15. F. Benkhaldoun, I. Elmahi, S. Sari and M. Seaid, *Int. J. Numer. Meth. Fluids*, 72 (2013) 967-993.
16. F. Benkhaldoun, S. Daoudi, I. Elmahi and M. Seaid, *Appl. Numer. Math.*, 62 (2012) 1749-1766.
17. I. Elmahi, F. Benkhaldoun, R. Borghi and S. Raghay, *Combust. Theor. Model.*, 8 (2004) 789-809.
18. M.A. Garcia, M. Gonzalez, M. Espino Infantes and A. Sanchez-Arcilla, *Revista Internacional de Métodos Numéricos para Calculo y Deseno en Ingenieria*, 11 (1995) 383-400.

(2018) ; <http://www.jmaterenvirosci.com>